Topological Mott Insulators

S. Raghu,[1] Xiao-Liang Qi,[1] C. Honerkamp,[2] and Shou-Cheng Zhang[1]

[1]*Department of Physics, McCullough Building, Stanford University, Stanford, California 94305-4045, USA*
[2]*Theoretical Physics, Universität Würzburg, D-97074 Würzburg, Germany*
(Received 10 October 2007; published 15 April 2008)

We consider extended Hubbard models with repulsive interactions on a honeycomb lattice, and the transitions from the semimetal to Mott insulating phases at half-filling. Because of the frustrated nature of the second-neighbor interactions, topological Mott phases displaying the quantum Hall and the quantum spin Hall effects are found for spinless and spin fermion models, respectively. The mean-field phase diagram is presented and the fluctuations are treated within the random phase approximation. Renormalization group analysis shows that these states can be favored over the topologically trivial Mott insulating states.

Introduction.—Partly motivated by the discovery of the high T_c superconductivity, the study of Mott insulators has attracted great attention in recent years. Defined in a general sense, interactions drive a quantum phase transition from a metallic to an insulating ground state in these systems. Most Mott insulators found in nature also have conventional order parameters, describing, for example, the charge-density-wave (CDW) or the spin-density-wave (SDW) orders. However, Mott insulators with exotic ground states, such as the current carrying ground states have also been proposed theoretically [1–4]. In parallel with the study of strongly correlated systems, there has recently been a growing interest in realizing topologically nontrivial states of matter in band insulators. In the quantum anomalous Hall (QAH) insulator [5,6], the ground state breaks time-reversal symmetry but does not break the lattice translational symmetry. The ground state has a bulk insulating gap, but has chiral edge states. In the quantum spin Hall (QSH) insulator [7–9], the ground state does not break time-reversal symmetry, has a bulk insulating gap, but has helical edge states, where electrons with the opposite spins counterpropagate. The QSH state has recently been predicted theoretically [9] and observed experimentally in HgTe quantum wells [10].

Given the tremendous interest in finding Mott insulators with exotic ground states, and the recent discovery of the topologically nontrivial band insulators, it is natural to ask whether one can find examples of topological Mott insulators, which we define as states with bulk insulating gaps driven by the interaction, and inside which lie topologically protected edge states. Furthermore, electronic states in the Mott insulator phases are characterized by topological invariants, namely, the $U(1)$ Chern number [11] in the case of the QAH state, and the Z_2 invariant [12] in the case of the QSH state. In this Letter, we report on the first example of such a case by systematically studying Hubbard models with repulsive interactions on a two-dimensional honeycomb lattice. The repulsive honeycomb Hubbard model was studied in the context of antiferromagnetism using quantum Monte Carlo simulations [13]

and is also a possible model for a spin liquid [14]. Here, we consider further neighbor repulsion and demonstrate that topological Mott phases displaying the QAH and the QSH effects are generated dynamically in this system.

Spinless fermions and the QAH state.—The model Hamiltonian for spinless fermions with nearest-neighbor and next-neighbor interactions is written as

$$H = -\sum_{\langle ij \rangle} t(c_i^\dagger c_j + \text{H.c.}) + V_1 \sum_{\langle i,j \rangle} (n_i - 1)(n_j - 1)$$
$$+ V_2 \sum_{\langle\langle i,j \rangle\rangle} (n_i - 1)(n_j - 1) - \mu\left(\sum_i n_i - N\right), \quad (1)$$

where V_1 and V_2 are nearest-neighbor and next-neighbor repulsions, respectively. Since the honeycomb lattice is bipartite, consisting of two triangular sublattices (referred to here as A and B), nearest-neighbor repulsion will favor a CDW phase with an order parameter $\rho = \frac{1}{2} \times (\langle c_{iA}^\dagger c_{iA} \rangle - \langle c_{iB}^\dagger c_{iB} \rangle)$ that breaks a discrete (inversion) symmetry. However, since the second-neighbor interactions within the same sublattice are frustrated, CDW order will
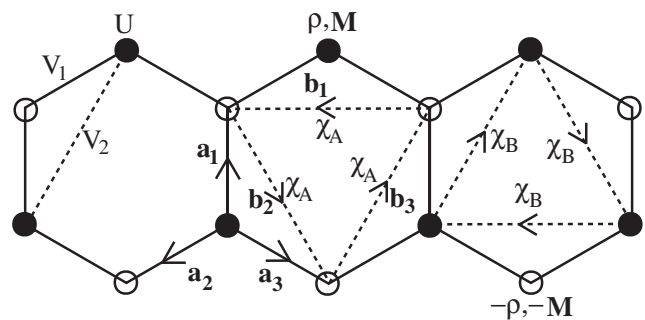

FIG. 1. Interactions considered in our model Hamiltonian (leftmost plaquette), Eq. (1). Various order parameters are shown for the A sublattice (open circles) and for the B sublattice (filled circles) in the middle and right plaquettes. The QAH-QSH order parameters χ_A, χ_B are complex 4-vectors associated with the directed second-neighbor links defined by $\boldsymbol{b}_i$. In the case of spinless fermions, χ_A and χ_B are complex scalars.

be suppressed; instead, we consider the possibility of generating bond order by defining the following order parameter for i, j next nearest neighbors: $\chi_{ij} = \chi^*_{ji} = \langle c^\dagger_i c_j \rangle$. Let a_1, a_2, a_3 be the nearest-neighbor displacements from a B site to an A site such that $z \cdot a_1 \times a_2$ is positive. We also define the displacements $b_1 = a_2 - a_3$, $b_2 = a_3 - a_1$, etc., which connect two neighboring sites on the same sublattice (Fig. 1). A translational and rotational invariant ansatz of χ_{ij} is chosen as

$$\chi_{i,i+\mathbf{b}_s} = \begin{cases} \chi_A = |\chi|e^{i\phi_A}, & i \in A \\ \chi_B = |\chi|e^{i\phi_B}, & i \in B \end{cases}, \quad (2)$$

which are complex scalars that live along the directed second-neighbor links. The real and imaginary parts of χ_{ij} break different discrete symmetries and are thus distinct order parameters: $\mathrm{Re}(\chi_{ij})$ breaks particle-hole symmetry, $\mathrm{Im}(\chi_{ij})$ breaks time-reversal symmetry, and both break the C_{6v} point-group symmetry when $\phi_A + \phi_B \neq 0$.

Because of translational symmetry, the mean-field free-energy at $T = 0$ is readily obtained:

$$F(\rho, \chi, \bar{\phi}, \phi) = -\sum_k \sqrt{|t(k)|^2 + (V_1\rho + 2V_2|\chi|S_{k+\bar{\phi}}S_\phi)^2}$$
$$+ 3L^2(V_1\rho^2 + 2V_2|\chi|^2). \quad (3)$$

Here, $t(k) = \sum_{n=1}^3 \exp(ik \cdot a_n)$, $\bar{\phi} = (\phi_A + \phi_B)/2$, $\phi = (\phi_A - \phi_B)/2$, $S_{k+\bar{\phi}} = \sum_{n=1}^3 \sin(k \cdot b_n + \bar{\phi})$, $S_\phi = \sin\phi$. Thus, the next-neighbor hopping amplitudes are purely real only when both $\phi = 0$ and $\bar{\phi} = 0$.

When both ρ and $\chi = 0$, and at half-filling, the system is a semimetal with two Fermi points $K_\pm$ that obey $K_\pm \cdot b_i = \pm 2\pi/3$ and the density of states vanishes linearly; the dispersion in the vicinity of these so-called Dirac points is governed by a 2D massless Dirac Hamiltonian in k space. The CDW phase corresponds to an ordinary insulator with a gap at the Fermi energy. As for χ, its phase relative to the nearest-neighbor hopping amplitude plays an important role in determining its properties: while a nonzero $\mathrm{Re}(\chi)$ merely shifts the energy of the Dirac points, a nonzero imaginary part $\mathrm{Im}(\chi)$ opens a gap at the Fermi points. Thus, when the system remains at half-filling, it is more favorable to develop purely imaginary next-neighbor hopping amplitudes; such a configuration corresponds to a phase with spontaneously broken time-reversal symmetry.

To see whether such a phase can be favored, we minimize the free-energy and arrive at the following self-consistent equations:

$$\rho = \frac{1}{6L^2} \sum_k \frac{V_1\rho + 2V_2\chi S_{k+\bar{\phi}}S_\phi}{\sqrt{|t(k)|^2 + (V_1\rho + 2V_2\chi S_{k+\bar{\phi}}S_\phi)^2}}, \quad (4)$$

$$\chi = \frac{S_\phi}{6L^2} \sum_k \frac{S_{k+\bar{\phi}}(V_1\rho + 2V_2\chi S_{k+\bar{\phi}}S_\phi)}{\sqrt{|t(k)|^2 + (V_1\rho + 2V_2\chi S_{k+\bar{\phi}}S_\phi)^2}}. \quad (5)$$

Because of the vanishing density of states near the Fermi

points, there is no instability towards any order with infinitesimal interactions. Interestingly, the self-consistent equation for χ shows that a nontrivial solution can occur only when $\phi \neq 0$, when $V_1 = 0$, beyond a critical value of $V_{2c} > 0$, which satisfies

$$\frac{1}{V_{2c}} = \frac{S_\phi^2}{3L^2} \sum_k \frac{S_{k+\bar{\phi}}^2}{|t_k|}, \quad (6)$$

a phase in which $|\chi| > 0$, $\bar{\phi} = 0$, and $\phi = \pm\pi/2$ is favored. Thus, the system acquires purely imaginary second-neighbor hoppings and breaks time-reversal symmetry. In the vicinity of this saddle point, fluctuations in both $\bar{\phi}$ and ϕ are gapped. This configuration is stable at finite V_1 and thus does not require fine-tuning (see Fig. 2). The band insulator version of the CDW state was considered in Ref. [15], while the quantum Hall (QH) state on a honeycomb lattice was considered in Ref. [5]. The phase with nonvanishing imaginary χ is precisely equivalent to the model in Ref. [5]. In this phase, the filled band has a nonzero Chern number [11] and is an integer quantum Hall effect phase that is realized without Landau levels [5]. QH states without Landau levels are referred to here as the QAH states. However, the topologically nontrivial gap for the QAH state arises here from many-body interactions, and we shall refer to such states as topological Mott insulators.

The mean-field phase diagram is shown in Fig. 2. There is a continuous transition from the semimetal to either the CDW or the QAH phase, and there is also a first-order transition from the CDW to the QAH phase that terminates at a bicritical point. By integrating out the fermionic fields, it is possible to construct a Landau-Ginzburg (LG) theory near the semimetallic region. Because of the linear dispersion of the Fermi points, the LG free-energy contains anomalous terms of the form $|\rho|^3$ and $|\mathrm{Im}(\chi)|^3$ [16]. Thus, even within mean-field theory, the CDW order pa-

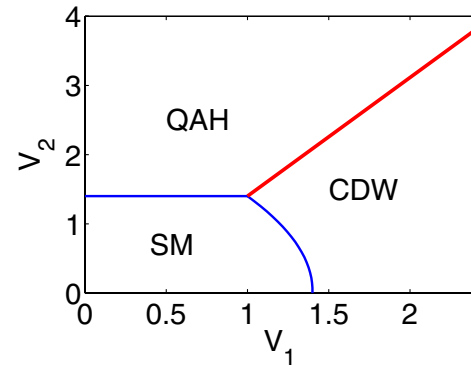FIG. 2 (color online). Phase diagram for spinless fermions ($t = 1$). The semimetallic (SM) state that occurs at weak coupling is separated from the CDW and the topological QAH states via a continuous transition. The line separating the QAH and CDW marks a first-order transition, which terminates at a bicritical point.

rameter, for instance, grows as $(V_1 - V_{1c})$ rather than the usual $(V_1 - V_{1c})^{1/2}$ [13].

Spinful fermions and the QSH state.—Next, we take into account the spin degrees of freedom and include an on-site Hubbard repulsion in our model Hamiltonian ($\mu = 0$):

$$H = -\sum_{\langle ij \rangle \sigma} t(c_{i\sigma}^\dagger c_{j\sigma} + \text{H.c.}) + U\sum_i n_{i\uparrow} n_{i\downarrow}$$
$$+ V_1 \sum_{\langle i,j \rangle} (n_i - 1)(n_j - 1) + V_2 \sum_{\langle\langle i,j \rangle\rangle} (n_i - 1)(n_j - 1), \quad (7)$$

where $n_i = n_{i\uparrow} + n_{i\downarrow}$. Since the honeycomb lattice is bipartite, on-site repulsion gives rise to a SDW phase at half-filling; a standard decomposition of the Hubbard term introduces the SDW order parameter $\boldsymbol{M}$: $\boldsymbol{M} = \frac{1}{2}(\langle \boldsymbol{S}_{iA} \rangle - \langle \boldsymbol{S}_{iB} \rangle)$. As in the spinless case, nearest-neighbor repulsion favors a CDW. Since the second-neighbor repulsion is frustrated, we are again led to the possibility of a topological phase similar to the QAH. However, the spin degrees of freedom introduce two possibilities (translation invariance along with spin conservation eliminate other possibilities): (1) two copies of QAH states—i.e. the chirality of the second-neighbor hopping is the same for each spin projection, (2) the QSH state, where the chiralities are opposite for each spin projection. The latter possibility breaks a continuous global $SU(2)$ symmetry associated with choosing the spin projection axis; however, time-reversal symmetry is preserved. The QSH state on the honeycomb lattice was considered in Ref. [7], where the insulating gap arises from the microscopic spin-orbit coupling. It was later shown that the magnitude of the spin-orbit gap is negligibly small in graphene [17,18]. In our case, however, the insulating gap is generated dynamically from the many-body interaction and can be viewed as an example of dynamic generation of spin-orbit interaction [19]. Introducing the Hubbard-Stratonovich fields (sum over repeated indices implied) $\chi_{ij}^\mu = c_{i\alpha}^\dagger \sigma_{\alpha\beta}^\mu c_{j\beta}$, $\mu = 0, \ldots, 3$, where $\sigma^\mu = (1, \boldsymbol{\sigma})$, the next-neighbor interactions can be recast using the identity $(n_i - 1)(n_j - 1) = 1 - \frac{1}{2}(\chi_{ij}^\mu)^\dagger \chi_{ij}^\mu$. Physically, $\langle \chi^0 \rangle \neq 0$ corresponds to the QAH phase, whereas if one of the vector components $\langle \chi^i \rangle \neq 0$, then the QSH phase occurs. A translationally invariant decomposition of the next-neighbor interactions via $\langle \chi_{i,i+\boldsymbol{b}_s}^\mu \rangle = \chi^\mu e^{i\phi_A^\mu}$, $i \in A$ (and similarly for the other sublattice) gives rise to a 4×4 Hamiltonian that is readily diagonalized in a tensor product basis $\boldsymbol{\sigma} \otimes \boldsymbol{\tau}$, where $\boldsymbol{\sigma}$ and $\boldsymbol{\tau}$ are Pauli matrices in spin and sublattice space, respectively. This way, each phase corresponds to a particular nonzero expectation value of a fermion bilinear $\sum_{\vec{k}} \Psi_{\vec{k}}^\dagger \hat{d}(\vec{k}) \Psi_{\vec{k}}$, where $\hat{d}(\vec{k}) \propto \tau^3$ for the CDW and QAH, and $\hat{d}(\vec{k}) \propto \sigma^3 \tau^3$ for SDW and QSH. A detailed and standard numerical study of the free-energy at $T = 0$ and its saddle point solutions produces the phase diagram shown in Fig. 3. In addition to the ordinary CDW and SDW insulating phases, there is a phase for $V_2 > V_{2c} \approx 1.2t$ in

which the 4-vector is purely imaginary (as in the spinless case), collinear, and staggered from one sublattice to the next: $\langle \chi_{ii+\boldsymbol{b}_n,A}^\mu \rangle = -\langle \chi_{ii+\boldsymbol{b}_n,B}^\mu \rangle$, and both QAH and QSH are equally favorable ground states, having identical free energies within mean-field theory. Additionally, there is never a coexistence of both QAH and QSH phases; indeed, a Landau-Ginzburg treatment in this region explicitly shows the absence $SO(4)$ symmetry of the vector χ^μ. This occurs due to the difference of the manner in which χ^0 and $\vec{\chi}$ are coupled to the fermionic fields—which favors either a phase with broken Z_2 symmetry (QAH) or with broken $SU(2)$ symmetry, but never both simultaneously [16].

Quantum fluctuations, however, lift the mean-field degeneracy between the QAH and QSH phases. To quadratic order in quantum fluctuations (RPA) about the QSH phase, we obtain an effective action $S_{\text{eff}} = \sum_{\vec{k}} \delta\chi^\mu(\vec{k}, \Omega) K_{\mu\nu}(\vec{k}, \Omega) \delta\chi^\nu(-\vec{k}, -\Omega)$, which shows the presence of six modes (2 longitudinal and 4 transverse modes), and 2 of the transverse modes correspond to degenerate Goldstone modes whose dispersion is given by $\Omega(\boldsymbol{q}) = \sqrt{|t_{k+q}|^2 - |t_k t_{k+q}|}$, which for $\boldsymbol{q}$ small is linear with velocity $\upsilon \approx \upsilon_f = 3t/2|\boldsymbol{a}|$. Thus, the zero-point motion associated with these gapless modes lowers the free-energy of the QSH state relative to the QAH state. In the presence of spin-orbit coupling (SOC), considering for concreteness the Rashba SOC $H_R = \lambda_R(\boldsymbol{s} \times \boldsymbol{p}) \cdot \hat{z}$, the Goldstone modes become gapped and do not interfere with the gapless edge excitations. Thus, by breaking the $SU(2)$ spin symmetry, the Rashba term stabilizes the QSH phase by ensuring that the only low energy excitations in the system are the helical edge modes of the QSH phase.

Renormalization Group Analysis.—Next, we go beyond mean-field theory and RPA using the temperature (T)-flow functional renormalization group (fRG)[20]. In this scheme, we discretize the $\vec{k}$- dependence of the interaction [21] and consider all possible scattering processes between a set of initial and final momenta that occur between points
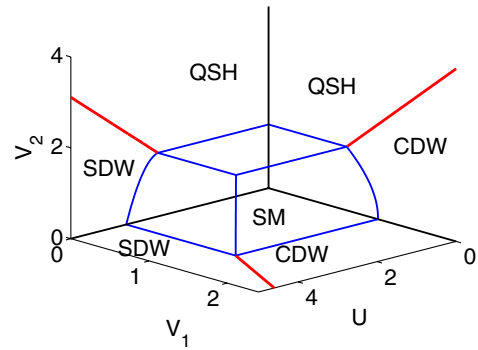

FIG. 3 (color online). Complete mean-field phase diagram for the spinful model. The transitions from the semimetal (SM) to the insulating phases are continuous, whereas transitions between any two insulating phases are first order.
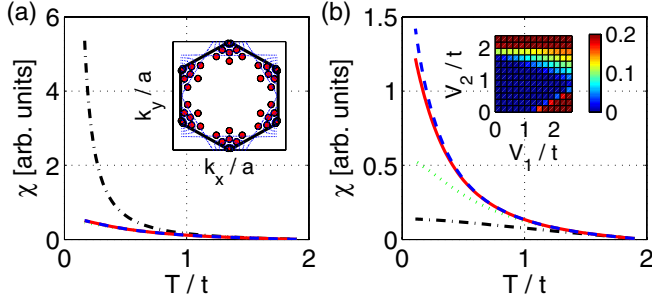
FIG. 4 (color online).   (a) Data for $U = 0$, $V_1 = 1.4t$, $V_2 = 0$. Susceptibilities of each phase vs T are shown: CDW (dash-dotted line); SDW (dotted line); QAH (solid line); and QSH (dashed line). (b) Same for $U = 0$, $V_1 = 0$, $V_2 = 1.8t$ (QSH instability). The QSH phase has a larger susceptibility than QAH. Inset: fRG phase diagram at $U = 0$, indicating SM and insulating regions (CDW dominates at large V_1, QSH at large V_2). The color bar corresponds to T_c below which the insulating phases develop in fRG.

on rings around the Dirac points (inset of Fig. 4). As the temperature T is lowered, a renormalized interaction V_T is obtained by the coupled summation of the T derivatives of all one-loop channels. Therefore, the method is unbiased and goes beyond mean-field theory. An ordering tendency at a finite vector $\boldsymbol{Q}$ can be detected as a growth of the associated vertex V_T. However, we have found that largest couplings occur at $\boldsymbol{Q} = 0$, which strongly supports the mean-field results presented above.

For on-site and nearest-neighbor repulsions $U > U_c \approx 3.8t$ and $V_1 > V_{1c} \approx 1.2t$, the flow to strong coupling is either an SDW instability for dominant U or a CDW instability for dominant V_1, in good agreement with a $1/N$ study [22] and quantum Monte Carlo calculations [13,23]. If we include a sufficiently strong second-neighbor repulsion $V_2 > 1.6t$, there is a leading growth of the QSH susceptibility. In Figs. 4(a) and 4(b) we compare the T flows of various susceptibilities for $V_1 > V_2$ and for $V_2 > V_1$. For the latter case, the QSH susceptibility grows most strongly toward low T, followed by the QAH susceptibility, which is consistent with the RPA treatment of the Goldstone modes in the QSH. The QSH phase remains stable even when a moderate on-site interaction of $U = t$ or $U = 2t$ is introduced. Hence the global structure of the mean-field phase diagram is confirmed by the fRG results.

Discussion.—We have shown that topological phases displaying the QAH and QSH effects can be generated from strong interactions—thus, we refer to these phases as topological Mott insulators. Both phases are described by conventional order parameters that develop continuously at the quantum critical phase transition from the semimetallic state. However, these states are also described by topological quantum numbers, which jump discontinuously at the transition.

While the topological Mott phases are unlikely to occur in graphene, the regime $V_2 > V_1$, U, where these phases are likely to occur, could equivalently be realized in a triangular optical lattice bilayer of dipolar atoms. By applying a static electric field to control the dipoles [24] and by varying the spacing between the layers, it is possible to tune the interactions such that $V_2 > U$, V_1; details will be provided elsewhere [16].

Interesting open issues include understanding coupling of the gapless bulk Goldstone modes with the gapless edge degrees of freedom, and the possibility of fractionalized excitations in these phases.

[1] I. Affleck and J. B. Marston, Phys. Rev. B **37**, 3774 (1988).
[2] X.-G. Wen and P. A. Lee, Phys. Rev. Lett. **76**, 503 (1996).
[3] C. M. Varma, Phys. Rev. Lett. **83**, 3538 (1999).
[4] S. Chakravarty, R. B. Laughlin, D. K. Morr, and C. Nayak, Phys. Rev. B **63**, 094503 (2001).
[5] F. D. M. Haldane, Phys. Rev. Lett. **61**, 2015 (1988).
[6] X. L. Qi, Y. S. Wu, and S. C. Zhang, Phys. Rev. B **74**, 085308 (2006).
[7] C. L. Kane and E. J. Mele, Phys. Rev. Lett. **95**, 226801 (2005).
[8] B. A. Bernevig and S. C. Zhang, Phys. Rev. Lett. **96**, 106802 (2006).
[9] B. A. Bernevig, T. L. Hughes, and S. C. Zhang, Science **314**, 1757 (2006).
[10] M. Konig, S. Wiedmann, C. Brune, A. Roth, H. Buhmann, L. Molenkamp, X.-L. Qi, and S.-C. Zhang, Science **318**, 766 (2007).
[11] D. J. Thouless, M. Kohmoto, M. P. Nightingale, and M. den Nijs, Phys. Rev. Lett. **49**, 405 (1982).
[12] C. L. Kane and E. J. Mele, Phys. Rev. Lett. **95**, 146802 (2005).
[13] S. Sorella and E. Tosatti, Europhys. Lett. **19**, 699 (1992).
[14] M. Hermele, Phys. Rev. B **76**, 035125 (2007).
[15] G. Semenoff, Phys. Rev. Lett. **53**, 2449 (1984).
[16] S. Raghu *et al.* (to be published).
[17] H. Min, J. E. Hill, N. A. Sinitsyn, B. R. Sahu, L. Kleinman, and A. H. MacDonald, Phys. Rev. B **74**, 165310 (2006).
[18] Y. Yao, F. Ye, X.-L. Qi, S.-C. Zhang, and Z. Fang, Phys. Rev. B **75**, 041401(R) (2007).
[19] C. Wu and S.-C. Zhang, Phys. Rev. Lett. **93**, 036403 (2004).
[20] C. Honerkamp and M. Salmhofer, Phys. Rev. B **64**, 184516 (2001); Phys. Rev. Lett. **87**, 187004 (2001).
[21] D. Zanchi and H. J. Schulz, Phys. Rev. B **61**, 13609 (2000).
[22] I. F. Herbut, Phys. Rev. Lett. **97**, 146401 (2006).
[23] C. Honerkamp (to be published).
[24] T. J. Carroll, K. Claringbould, A. Goodsell, M. J. Lim, and M. W. Noel, Phys. Rev. Lett. **93**, 153001 (2004).